Computer Modeling in Engineering & Sciences

Tech Science Press

https://doi.org/10.32604/cmes.2026.080371

ARTICLE

Compression vs. Tension-Induced Wrinkle Formation on Thin Film Structures: Three-Dimensional Numerical Simulations

Md Al Rifat Anan[1], **Donghyeon Ryu**[2] **and Yu-Lin Shen**[1,*]

[1]Department of Mechanical Engineering, University of New Mexico, Albuquerque, NM, USA
[2]Department of Mechanical Engineering, New Mexico Institute of Mining and Technology, Socorro, NM, USA

*Corresponding Author: Yu-Lin Shen. Email: shenyl@unm.edu

Received: 08 February 2026; Accepted: 08 April 2026; Published: 27 May 2026

ABSTRACT: The development of surface wrinkles on thin films bonded to compliant substrates is recognized as a form of mechanical instability. While this wrinkling behavior is widely studied when the thin film is under direct compression, much less attention has been devoted to the prediction of wrinkle formation caused by tension and cyclic compression-tension deformations. This work focuses on compression vs. tension-induced wrinkles using a relatively stiff polymeric film on an elastomeric substrate as the model system. Experimental observations show that parallel wrinkles formed during unidirectional compression gradually disappear under reverse loading. When the thin film structure is pulled into tension, a new set of parallel wrinkles in the perpendicular direction would develop. The tension-induced wrinkles are caused by Poisson's ratio mismatch between the film and substrate, which generates lateral compression in the film. By way of the embedded imperfection technique in three-dimensional (3D) finite element modeling, we illustrate that this type of wrinkle transition can be simulated in a seamless manner. With the linear elastic assumption, the overall load-displacement response and evolution of wrinkles are shown to be reversible. The tension-after-compression and direct tension loading conditions lead to exactly the same material response, including the deformation instability. Further analyses on the effects of film modulus and Poisson's ratio are performed, with the differences in wrinkling behavior under compressive and tensile loading contrasted.

KEYWORDS: Instability; wrinkle; stiffness; reversibility; cyclic loading

1 Introduction

Mechanical instability in the form of surface wrinkles is of growing interest in modern technologies involving soft materials in thin-film substrate systems [1,2]. Surface wrinkles commonly exist in both natural and synthetic systems, e.g., constrained swelling hydrogels under environmental stimuli (e.g., pH, humidity, and temperature) [3–6], dried fruits and vegetables [7,8], and anatomical structures [9,10]. The wrinkling behavior depends on material properties, geometric configurations, boundary conditions, and mechanical forces such as compression, shear, pre-strain, swelling, drying, shrinking, applied voltage, and growth [11–15]. Under uniaxial or biaxial compression, a film-substrate structure may deform into various surface morphologies, e.g., sinusoidal [16–20], checkerboard [21–24], hexagonal [22–25], herringbone [21,23,25,26], and labyrinth [21,26] patterns or period-doubling wrinkles and folds [27–31]. These complex features are a direct mechanical response when the deformation of the thin film reaches a critical level [32,33]. Predicting wrinkle inception and its evolution is important for applications in adhesion, wettability, and other functionalities [34–37]. Although wrinkle formation is traditionally considered an undesired surface deformation,

in recent years, wrinkling has also emerged as a viable mechanism to improve device performance in advanced technology. Its controlled application is now key for the development of stretchable electronics [38–42], sensor development [43,44], smart medical devices [45–47], and functional surfaces [48–52] with tailored properties.

For structures consisting of a stiff thin film bonded to a compliant substrate, surface wrinkling is generally dictated by the minimization of the total potential energy. Wrinkle formation releases a part of the elastic strain energy in the film but increases that of the substrate. Therefore, both the mechanical properties of the film and substrate contribute to the onset of instability. The role of linear elastic behavior in the wrinkling of film-substrate systems has been explored extensively [36,37,53–55]. In general, uniaxial compression beyond a threshold triggers the occurrence of sinusoidal wrinkles. This paradigm was clearly demonstrated in early studies on metal and oxide films on pre-tensioned elastomeric substrates [56,57]. Upon relaxation of the pre-strain, elastic recovery of the substrate exerts a compressive stress state on the confined film. When it exceeds the critical buckling strength, the flat and uniform state becomes mechanically unstable and bifurcates into a periodic out-of-plane undulated low-energy state [58,59]. This simple concept has been developed into a metrological technique for the extraction of thin film modulus, adhesion energy, and fracture toughness [60]. The transition of wrinkles, for instance, from the sinusoidal mode to period-doubled, herringbone-like, or localized ridge forms, introduces further complexity involving the constitutive behavior of the film-substrate layers [61–63].

While numerous foundational studies have generated insights into instabilities in thin-film systems, a direct comparison of loading pathways has not been well studied. Jiang et al. [64] investigated the post-buckling behavior of thin film on a pre-tensioned and subsequently compressed substrate, analyzing the resulting changes in amplitude and wavelength of the wrinkles. Wang and Zhao [63] mapped out the instability phase diagram of extended systems by the pre-stretch/release technique. Arafat et al. [65] investigated the relationship between cracking, delamination, and buckling for thin metallic films on elastomers under stretching. Lipomi et al. [66] developed stretchable structures based on compliant electrical conductors using wrinkling for strain accommodation under compression. Sekitani et al. [67] developed printable elastic conductors using single-walled carbon nanotubes in rubber for high conductivity and stretchability under tension. Generally speaking, attention has usually been placed on the functionalities of the wrinkled state instead of a mechanistic side-by-side comparison between deformation pathways (compression-tension).

The conducting polymer poly(3,4-ethylenedioxythiophene): poly(styrenesulfonate) (PEDOT:PSS) thin film deposited on the substrate of poly(dimethylsiloxane) (PDMS) elastomer is an ideal model system for investigating the mechanical instabilities from the perspective of organic stretchable devices [66]. PEDOT:PSS is typically glassy and has a much higher elastic modulus compared to PDMS which is very soft and stretchable [68,69]. Such a large mechanical mismatch, with a modulus difference of several orders of magnitude, makes the system particularly prone to instability. Under compression, a well-adhered film can form ordered, reversible wrinkles. However, when stretched, the PEDOT:PSS film tends to form channel cracks, which can electrically isolate sections of the film and lead to device failure [65]. The interfacial adhesion energy is a dominant factor, governing whether the system relieves stress through conformal buckling, delamination, or film cracking [70,71]. Bi et al. [72] presented a numerical study on the dynamic wrinkling behavior of stiff film/compliant substrate structures, analyzing factors like pre-strain and substrate modulus on the system's potential energy and dynamic response. Recent studies on the electromechanical coupling of such systems showed that, despite their reversible nature at moderate strains, mechanical instabilities can strongly affect electrical conductivity—improvement through wrinkling-driven alignment of conductive pathways or degradation by cracking [73,74]. Analytical as well as numerical models have been developed to predict these modes of buckling in such bilayers or tri-layers, thus establishing a strong connection between

observed morphologies and underlying material properties [75,76]. The particular pattern that occurs is very sensitive to the stress state (e.g., biaxial or uniaxial) as well as geometric confinement of the system [77]. Shan et al. [78] investigated wrinkling deformation of square films subjected to in-plane torsion revealing multiple wrinkling configuration transitions during evolution expanding beyond compression-tension. Yang et al. [79] showed that wrinkle wavelength decreases with increasing pre-strain, and uniform wrinkling occurs only within a specific range of yield properties—too low a yield stress suppresses wrinkling, while too high a yield stress leads to non-uniform patterns.

An embedded imperfection technique was recently developed to simulate wrinkle formation within the finite element modeling framework [80–83]. The temporal wrinkling evolution can be captured in a straightforward manner, and the methodology has been employed to study complex surface patterns in three-dimensional settings [84,85]. In contrast to the well-established compressive route, wrinkle formation under tensile strain involves a more complex and less explored mechanical pathway. When a film-substrate system is stretched, the initial response to the stretching is a uniform expansion. Beyond a critical strain, however, the system can bifurcate, leading to a variety of instabilities including sinusoidal wrinkles, delamination blisters, and counter-intuitive wrinkle-like patterns that form along the stretching direction [65,86,87]. Gao et al. [88] investigated a new wrinkling system where tension creates localized wrinkles near the edge of films on PDMS, offering insights into how tension drives wrinkling through different mechanisms from compression. Qiu et al. [89] presented an energy-based theory for stretch-induced wrinkling in rectangular films, and introduced power-law shape functions and energy barrier concepts to describe wrinkle bifurcation and evolution. While the thin film is stretched in one direction, the mismatch of Poisson's ratios between film and substrate may induce lateral compressive stress in the film, causing eventual wrinkle formation. The asymmetric behavior of thin films under compressive and tensile loading has not been systematically examined, and a unified modeling framework capturing both deformation modes is needed. The present work builds upon our previously developed embedded imperfection technique to numerically study the compression vs. tension-induced wrinkling instabilities, using the PEDOT:PSS thin film on PDMS substrate as a model system. It follows a continuum-based numerical approach using the finite element method, assuming a linear-elastic constitutive behavior. The specific objectives include:

- To demonstrate that the numerical approach is capable of predicting the transformation of parallel wrinkles from prior compressive loading into a new set of parallel wrinkles in the perpendicular direction under reversed tensile loading, as observed in experiments.
- To compare the instability behaviors caused by two different deformation histories—"tension after compression" and "direct tension."
- To examine the effects of the elastic modulus of the thin film on the wrinkle formation induced by compression and tension.
- To study how the difference in Poisson's ratio between the film and substrate affects the compression-induced and tension-induced wrinkles.

In the remainder of this paper, we first describe experimental observations in Section 2, which is followed by the numerical model description in Section 3. Section 4 includes the simulations of wrinkle transitions following the loading sequence used in the experiment, along with relevant discussion. Section 5 presents parametric numerical analyses on the film properties, to contrast their different influences on wrinkling induced by compression and tension. Important findings are summarized in Section 6.

2 Experimental Observation

The film-on-substrate structure was produced by spin-coating a PEDOT: PSS thin film onto the pre-fabricated and pre-stretched PDMS substrate. Relaxing the pre-tension effectively compresses the film, and

the critical state can be easily reached to trigger sinusoidal wrinkles. Subsequent pulling of the structure along the same direction essentially reduces the film compression and then moves further into the tensile regime. Fig. 1 shows the schematics based on the optical microscopic images of the wrinkles at different stages. In the relaxed state (most compressed), wrinkles are aligned in the direction perpendicular to the loading axis. As reversed deformation progresses, the compressive strain experienced by the film is reduced, and the wrinkles gradually flatten. A new set of wrinkles oriented along the tensile loading direction starts to take shape.

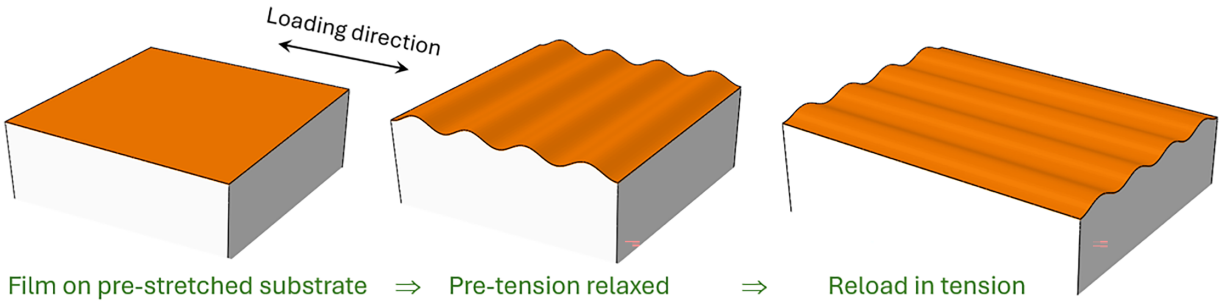

Figure 1: Schematics depicting the experimentally observed reversible wrinkle evolution in a film/substrate structure. The thin film was fabricated on a pre-stretched elastomeric substrate. Upon relaxation, the film was effectively under compression, forming wrinkles. The structure was reloaded back into tension and a new set of wrinkles parallel to the tensile direction was observed.

Although both the film and substrate are under horizontal tension at the later stages of the process, the greater tendency for PDMS to contract laterally (due to its higher Poisson's ratio than that of PEDOT:PSS) exerts an increasing compressive strain in the film along the perpendicular direction. Wrinkling thus develops in response to this lateral compression. This type of wrinkle transition due to cyclic compression-tension loading has also been reported in other experimental studies [39]. The numerical modeling presented below aims to capture the same process through 3D finite element analysis.

3 Numerical Model Description

The problem domain consists of a thin film above a compliant substrate with perfect bonding. As shown in Fig. 2, the film surface was square-shaped in the xz-plane. The film thickness is taken as 0.1 μm, and the substrate was sufficiently thick in comparison with the film (about 280 times thicker). The choice of dimensions in the x- and z-directions was guided by the theoretical critical wavelength under compression (see equation below), and they are taken as ten times the critical wavelengths to ensure a sufficient number of wrinkles once formed [85]. The computational domain serves as the 3D representative volume element of the larger periodic structure, minimizing boundary effects while maintaining computational efficiency. To help trigger instability, an embedded imperfection is included, which is a regular finite element at the center of the top-layer elements of the substrate (immediately below the film/substrate interface). Although this element is a part of the substrate, it is assigned the properties of the film material, so this arrangement may be viewed as having an interface that is not perfectly flat.

Fig. 2 also includes the boundary conditions. Two vertical side surfaces (an xy-plane and an yz-plane) are references planes, where out-of-plane movement is prohibited but tangential slides are allowed. Pushing and pulling displacements are imposed on the other yz-plane along the x-direction, with tangential slides allowed to simulate compressive and tensile loading, respectively. The remaining vertical side face, an xy-plane, can move in a parallel fashion and stays vertical and planar with tangential slides allowed. The

top surface of the film and the bottom surface of the substrate are traction-free. These conditions ensure a representative volume element within a large periodic system along the x- and z-directions [90].

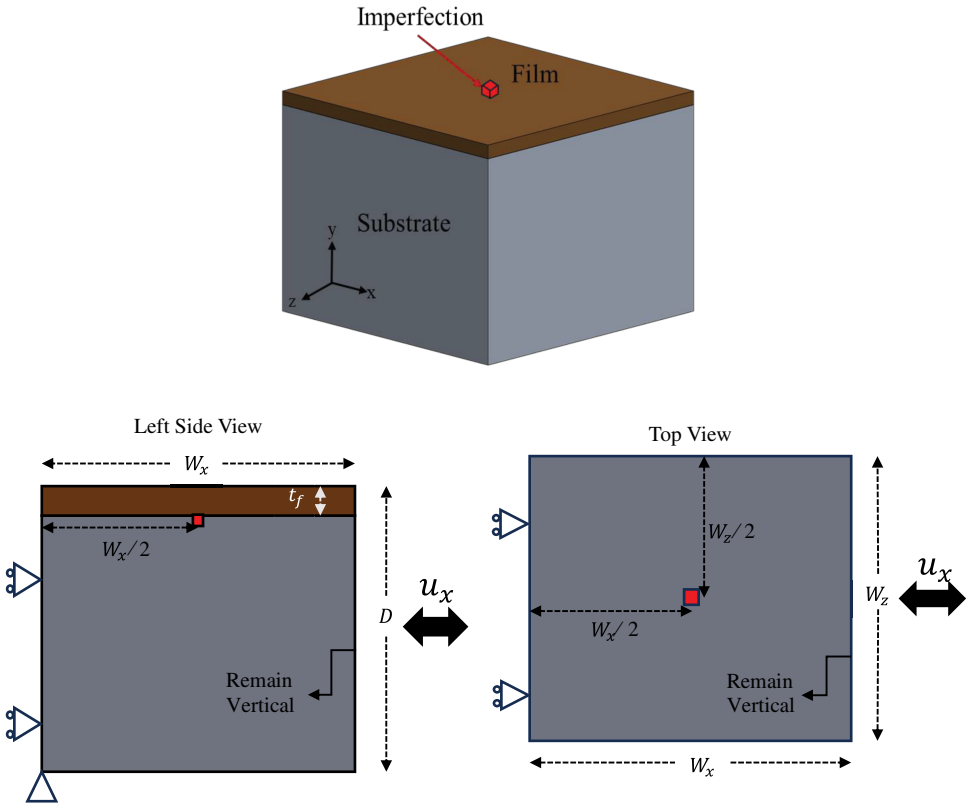

Figure 2: Schematics of the problem geometry, boundary conditions, and directions of the applied displacement. The model dimensions are: W_x = 37.2791 µm, W_y = 27.9593 µm, W_z = 37.2791 µm, t_f = 0.1 µm.

To establish a baseline and compare the numerical results with available analytical solutions, all materials are assumed to be isotropic and linearly elastic. The Young's modulus (E_f) and Poisson's ratio (v_f) of the PEDOT:PSS film are 2000 MPa and 0.35, respectively [91]. For the PDMS substrate, its Young's modulus (E_s) and Poisson's ratio (v_s) are 2.97 MPa and 0.495, respectively [91]. The simulations were carried out using the finite element program ABAQUS (Version 2022). The model employs 20-noded higher-order brick elements throughout, with a uniform mesh in the film layer consisting of four elements across its thickness. In the substrate, the mesh density was gradually reduced with depth to optimize computational efficiency while maintaining accuracy near the film-substrate interface. To ensure numerical convergence, an in-plane mesh density equivalent to ten elements per analytical sinusoidal wavelength is used, following established guidelines [84].

As described above, the overall model dimensions are scaled according to the theoretical critical wavelength corresponding to the primary sinusoidal buckling mode [59,92],

$$\lambda_{cr} = 2\pi t_f \left[\frac{\left(1 - v_s^2\right) E_f}{3\left(1 - v_f^2\right) E_s} \right]^{\frac{1}{3}} \tag{1}$$

Note that this expression pertains only to compression following the plane strain assumption (or, using the current modeling scheme, no displacement allowed in the z-direction). Under the same condition, the critical stress at the onset of primary bifurcation, σ_{cr}, was analytically derived as [58,59,92]

$$\sigma_{cr} = \left[\frac{E_f}{4\left(1-{\nu_f}^2\right)}\right]\left[\frac{3\left(1-{\nu_f}^2\right)E_s}{\left(1-{\nu_s}^2\right)E_f}\right]^{\frac{2}{3}} \tag{2}$$

Dividing Eq. (2) by the plane strain modulus of the thin film, $\frac{E_f}{1-{\nu_f}^2}$, one obtains the critical wrinkling strain e_{cr} as

$$e_{cr} = \left(\frac{1}{4}\right)\left[\frac{3\left(1-{\nu_f}^2\right)E_s}{\left(1-{\nu_s}^2\right)E_f}\right]^{\frac{2}{3}} \tag{3}$$

Eq. (3) will be used below to validate our numerical models. There is no analytical solution for uniaxial compressive loading (non-plane-strain) and tensile loading. Predicting wrinkling instabilities therefore relies on numerical simulations.

4 Numerical Results: Compression Loading Followed by Tension

Fig. 3 shows the overall load-strain curve obtained from the finite element modeling of uniaxial compression from the initial stress-free state. Three points are labeled along the curve, with the corresponding snapshots of the model configuration also shown in the figure. At point A, the film-substrate structure is flat, and it remains flat under increasing compression throughout the beginning linear portion of the load-strain curve. There is a distinct change in slope at the strain of 0.00842, which marks the onset of surface wrinkling as the system bifurcates from a state of uniform compression to a periodized, out-of-plane buckling mode. Point B in Fig. 3 is shortly after this instability, and it can be seen that the wrinkling pattern has started to form. The wavelength and the evolution of amplitude have been shown to agree with established analytical solutions in our previous work [84]. With a greater compressive strain at point C, well developed sinusoidal wrinkles are observed. Upon unloading from point C, the overall load-strain response is fully retraced following the same path. The wrinkles gradually disappear and the structure becomes flat again after entering the pre-instability regime. The three simulation images can thus represent unloading history as well.

Fig. 4 shows the overall load-strain cyclic curve, starting from an initial flat and stress-free state (point A) into compression, with subsequent unloading and reversed loading into tension, following the history of A-X-A-B-C as labeled along the curve. Note that the A-X-A portion is the same as in Fig. 3 but it is repeated here for completeness. The surface patterns corresponding to points X, A, B and C are also shown in the figure. From X back to A, the compression-induced wrinkles vanish. Further loading leads to elastic stretching of the structure. The greater Poisson contraction of the substrate imposes lateral compression on the film. Upon reaching a critical tensile strain of 0.1712, the second instability commences in response to this lateral compression. A new set of wrinkles in the perpendicular direction, aligning with the tensile axis, takes shape. From B to C the wrinkles grow more prominent with a greater amplitude.

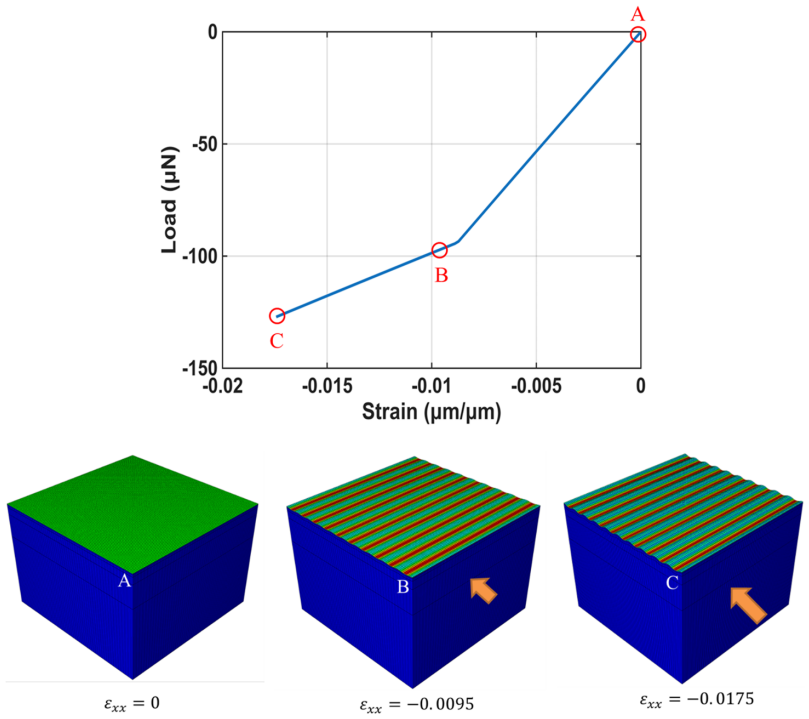

Figure 3: Uniaxial compression of the PEDOT: PSS/PDMS bilayer, showing the overall load-strain response and the progression of surface configuration from the undeformed to wrinkled states, corresponding to points A, B and C labeled along the curve.

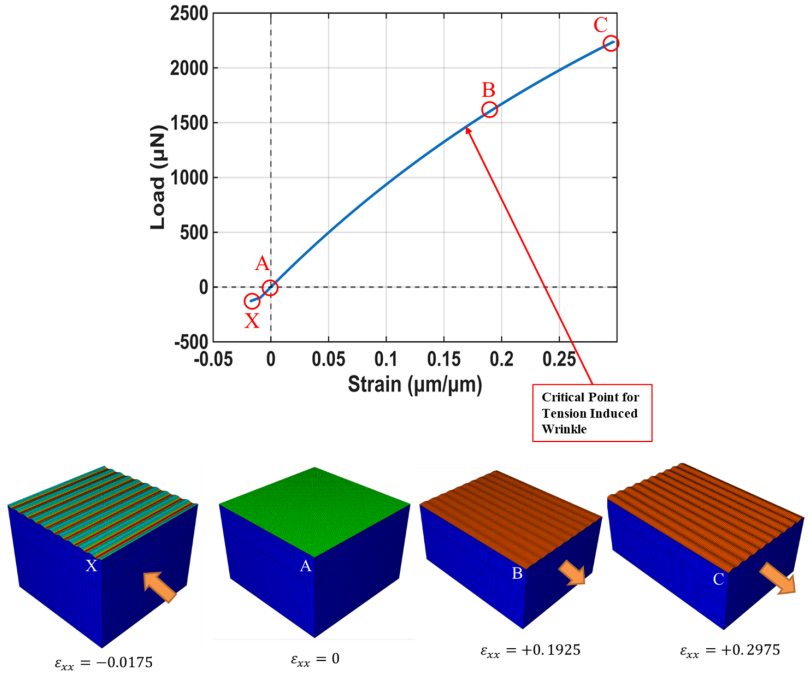

Figure 4: Cyclic load-strain response of the PEDOT: PSS/PDMS bilayer, starting with compression from points A to X, then unloading from X to A, and then further loading in tension through points B and C. Snapshots of surface morphology corresponding to points X, A, B and C, showing wrinkle transition, are included. Point B is shortly after the critical point for tension-induced instability.

The above results illustrate that the current modeling approach is able to capture the orientational transition of wrinkles due to loading in opposite directions, consistent with experimental observation [39]. Furthermore, the entire process is predicted using one smooth simulation run without any *ad hoc* treatment. The comparison of modeling with experiment is limited to qualitative features due to insufficient quantitative information of the actual measurement. It is also noted that the tensile strain to induce wrinkles seen in Fig. 4 is relatively large, which also implies nonlinear behavior in actual materials. The viscoelastic response, nonlinear elasticity (especially for the elastomeric substrate), plastic yielding of the film, and structural damage such as local interfacial delamination are all possible reasons contributing to the actual deformation behavior. The rate-dependent viscous effect will contribute significantly to relaxation and alter the stress state during both compression and tension. These will be left for future studies. The present work focuses on the straightforward elastic instability to demonstrate the model capability, establish fundamental characteristics of compression/tension wrinkle formation, and examine the effects of film/substrate elastic properties through parametric analyses.

A separate simulation is conducted, using only pure tensile loading directly from the initial stress-free state. The result is shown in Fig. 5 (as "pure tension"), along with the tensile portion of the load-strain curve in Fig. 4 ("tension after comparison") for comparison. The two curves coincide over the entire strain range. In addition, in both cases, the tension-induced wrinkles start to develop at the same strain (0.1712), and the wrinkle patterns are also identical (as the deformation images of points B and C shown in Fig. 4). Therefore, the tensile instability is unaffected by the prior deformation history.

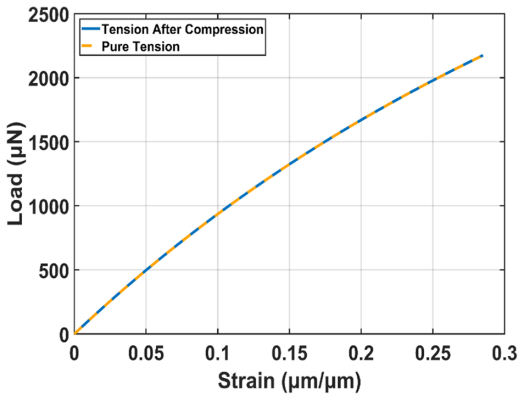

Figure 5: Comparison of load-strain responses for pure tension and tension applied after compression in the PEDOT:PSS/PDMS structure. The overlapping curves indicate reversible deformation behavior, showing that prior compression and wrinkle formation do not affect the tensile response.

5 Numerical Results: Parametric Analyses of Film Properties

5.1 Effect of Film Modulus

In this section, we present simulation results based on various Young's moduli of the thin film, to examine how the wrinkling behavior may be affected in compression and in tension. The film modulus considered ranges from 2000 to 6000 MPa, while the substrate modulus is kept unchanged at 2.97 MPa. Owing to the deformation path independence reported above, only direct compression and direct tension are considered without any prior history. Fig. 6 shows the compressive critical strain for wrinkle formation as a function of film/substrate modulus ratio (E_f/E_s). Two simulation results are included: one from uniaxial compression and one from plane-strain compression. The latter was implemented by fixing the model dimension in the z-direction while compression in x is applied. Also included in the figure is the analytical

curve following Eq. (3) which is based on the plane strain condition. It is evident that the plane-strain simulation curve matches the analytical solutions throughout the range of E_f/E_s. The critical compressive strain decreases as E_f/E_s increases, indicating that stiffer films wrinkle more easily. This occurs because a higher stiffness mismatch leads to the film experiencing a greater share of stress, causing the system to relieve strain energy through earlier out-of-plane buckling. Fig. 6 also illustrates that, under uniaxial compression, the critical strains are consistently greater than those under plane-strain compression. In uniaxial compression, the structure has the flexibility to expand laterally, which results in a delayed start of instability.

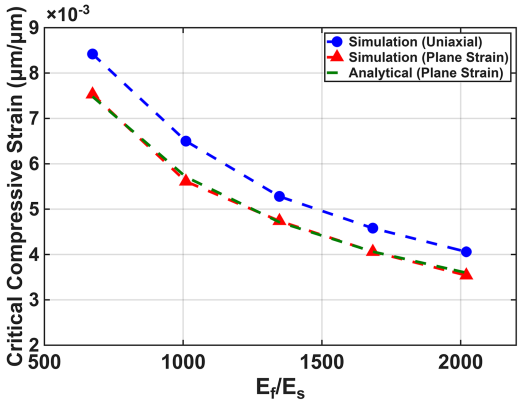

Figure 6: Critical compressive strain for wrinkle initiation as a function of the film/substrate modulus ratio. Two simulation curves are included: uniaxial compression and plane-strain compression. A curve based on the analytical expression of plane-strain compression, Eq. (3), is also shown for comparison.

Fig. 7 shows the variation of critical tensile strain with stiffness ratio E_f/E_s, for uniaxial tensile stretching obtained from the modeling. Note that there is no analytical solution available, and the plane strain condition is not applicable (by default, wrinkles are induced by lateral contraction). Compared to compression, the most apparent difference for tension is that the critical strain increases with E_f/E_s, meaning that stiffer films resist wrinkling. This is the opposite trend to the compression case. Under tensile loading, the lateral compression experienced by the film is caused by the contraction mismatch with the substrate. Therefore, for maintaining equilibrium, a stiffer film will be compressed less laterally under a fixed overall pulling strain. As a consequence, the onset of instability will be delayed.

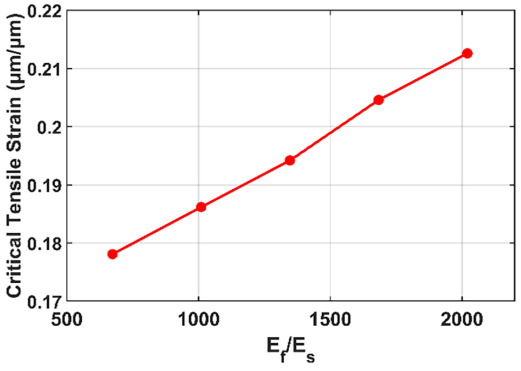

Figure 7: Critical tensile strain for wrinkle initiation as a function of the film/substrate modulus ratio, obtained from the simulations.

In the simulations, the surface deformation can be monitored, which provides the amplitude information once wrinkling commences during the compressive and tensile loading. Fig. 8a,b show the evolution of wrinkle amplitude as a function of applied compressive strain and tensile strain, respectively. Before the critical state, the amplitude stays at zero because the deforming structure is still flat. Upon reaching instability, the amplitude soon develops and the wrinkles take shape. In accordance with Figs. 6 and 7, the critical strain decreases and increases with an increasing film modulus for compressive loading and tensile loading, respectively. In general, compression-induced wrinkles initiate at a much smaller strain than tension-induced wrinkles. The amplitudes of compression-induced wrinkles also grow at a faster pace.

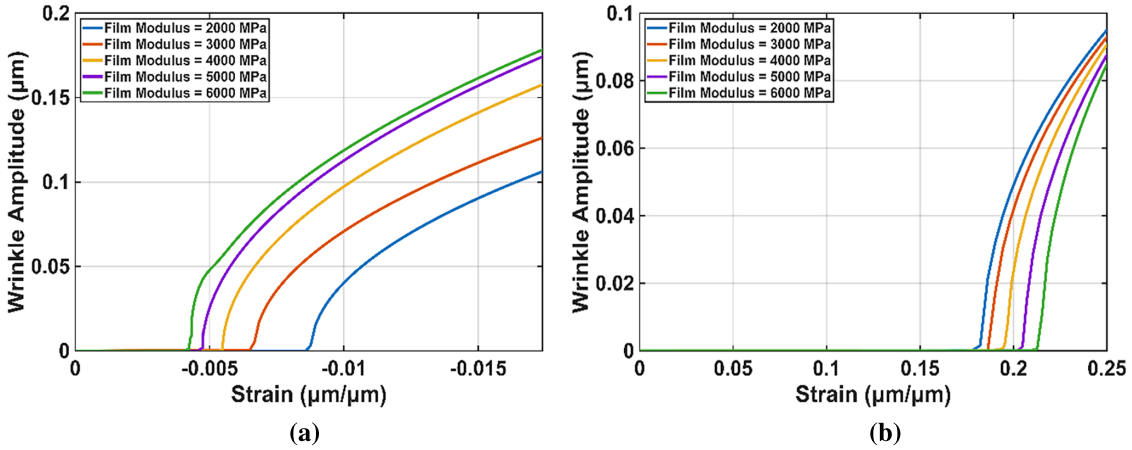

Figure 8: Evolution of wrinkle amplitudes as a function of the applied (**a**) compressive strain and (**b**) tensile strain. Results for five different elastic moduli of the thin film are included.

5.2 Effect of Poisson's Ratio

In addition to film modulus, another important elastic property to consider is Poisson's ratio, especially because tension-induced wrinkling is driven by the Poisson contraction mismatch. Here we vary the Poisson's ratio of the thin film between 0.15 and 0.4 while keeping the substrate Poisson's ratio at 0.495. Fig. 9 shows the critical compressive strain as a function of the difference in Poisson's ratio $(\nu_s - \nu_f)$, with two simulation curves (uniaxial compression and plane-strain compression) included, along with the analytical curve based on Eq. (3). Plane-strain compression obtained from modeling is again seen to agree with theoretical predictions. Uniaxial compression results in higher critical strains compared to plane-strain compression, since in uniaxial compression the structure has the ability to accommodate lateral expansion and thus delays the onset of buckling. Although there appears to be opposite trends for the variation of compressive critical strain under uniaxial and plane-strain deformation, the critical strain is relatively insensitive to $\nu_s - \nu_f$.

Fig. 10 shows the variation of critical tensile strain with the difference in Poisson's ratio. A very significant dependence is evident, with the greater Poisson mismatch $(\nu_s - \nu_f)$ leading to a sharply reduced critical strain. Earlier formation of wrinkles in the perpendicular orientation is thus predicted. If the difference between ν_s and ν_f is small, the lateral compressive stress in the film is difficult to build up, which delays instability, so the critical strain becomes high.

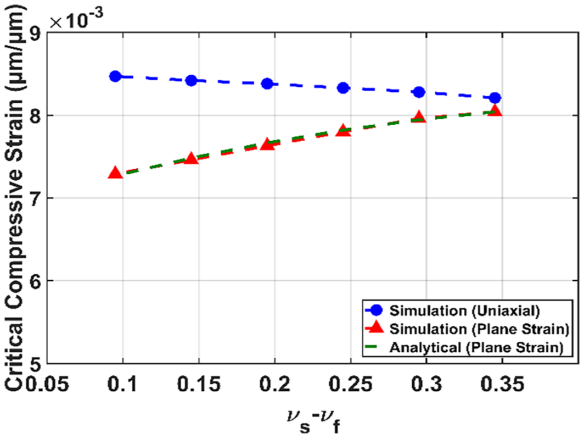

Figure 9: Critical compressive strain for wrinkle initiation as a function of the difference in Poisson's ratio $(\nu_s - \nu_f)$. Two simulation curves are included: uniaxial compression and plane-strain compression. A curve based on the analytical expression of plane-strain compression, Eq. (3), is also shown for comparison.

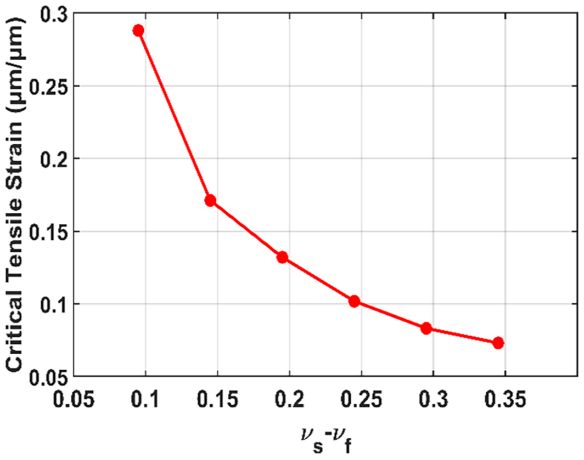

Figure 10: Critical tensile strain for wrinkle initiation as a function of the difference in Poisson's ratio $(\nu_s - \nu_f)$, obtained from the simulations.

Fig. 11a,b show the evolution of wrinkle amplitudes as a function of applied compressive strain and tensile strain, respectively, for six different values of Poisson's ratio of the thin film. Again, pre-instability deformation is represented by the portion of zero amplitude. In Fig. 11a, the six cases display close values of critical compressive strain (corresponding to Fig. 9). Their evolutions of amplitude are also very similar, confirming the insensitive nature to lateral Poisson contraction mismatch when wrinkling instability is a direct response to compressive loading. As for tensile loading, the large differences in the critical point among the cases of varying film Poisson's ratio can be easily seen in Fig. 11b. When ν_f is lower (e.g., 0.15), not only does wrinkling start earlier due to the greater lateral contraction mismatch, but the wrinkles also develop more rapidly with a greater slope in Fig. 11b. With an increasing ν_f (approaching ν_s), surface instability becomes more difficult to develop, thus demonstrating the critical role played by the Poisson's ratio mismatch in forming wrinkles induced by tensile loading.

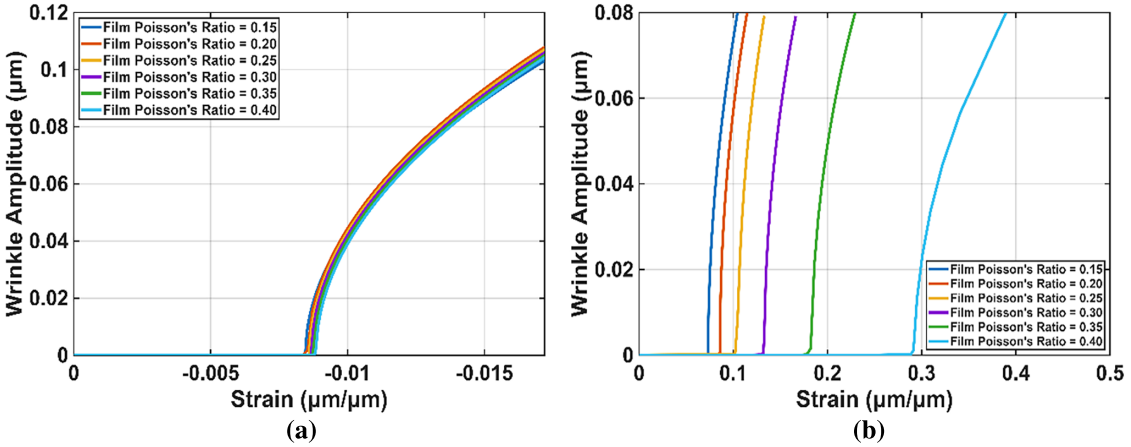

Figure 11: Evolution of wrinkle amplitudes as a function of the applied (**a**) compressive strain and (**b**) tensile strain. Results for six different Poisson's ratios of the thin film are included.

6 Conclusions

Numerical finite element analyses were conducted to simulate the wrinkling instabilities on the thin film-compliant substrate structure, induced by both compressive and tensile loading. The study is motivated by experimental observations that previously formed parallel wrinkles under compression gradually transform into a new set of parallel wrinkles in the perpendicular direction, as the structure is loaded in the reversed direction into tension. We demonstrate that this transition of wrinkle patterns during the compression-tension cycle can be obtained through the embedded imperfection technique using a single continuous simulation run. Wrinkling induced by tension is caused by the mismatch in Poisson contraction between the film and substrate, forcing the film into lateral compression, which can exceed the critical state as deformation continues. Due to the reversibility of elastic wrinkles, the histories of "tension after compression" and "pure tension" were found to generate the same overall deformation response. Parametric numerical analyses showed that an increasing film-to-substrate modulus ratio E_f/E_s leads to easier wrinkle formation under compression, but an opposite trend is true for tension. Tension-induced wrinkles are also heavily influenced by the difference in Poisson's ratio, with close values of ν_s and ν_f drastically increasing the difficulty of triggering instability. Compression-induced wrinkle formation, on the other hand, is insensitive to Poisson's ratio. The present study assumes linear elastic material behavior and perfect bonding between the film and substrate. Effects such as nonlinear elasticity, viscoelasticity, plastic deformation, potential interfacial damage, as well as film cracking under various loading conditions are not considered. Incorporating these effects, as well as further investigations of the multiaxial loading effect leading to complex surface patterns, will be explored in future analyses.

Acknowledgement: The authors acknowledge Siavash Nikravesh for his early foundational work leading to this study.

Funding Statement: The authors disclosed receipt of the following financial support for the research, authorship, and/or publication of this article: The authors would like to acknowledge NASA EPSCoR CAN (grant #: 80NSSC23M0069) for supporting this study. Yu-Lin Shen further acknowledges the endowment support from PNM Resources Foundation.

Author Contributions: Md Al Rifat Anan and Yu-Lin Shen conceived the idea for the research and contributed writing the first draft. Md Al Rifat Anan performed numerical simulations directed by Yu-Lin Shen. Donghyeon Ryu provided guidance on the physical behavior of materials. All authors reviewed and approved the final version of the manuscript.

Availability of Data and Materials: The datasets generated and analyzed during the current study are available from the corresponding author on reasonable request.

Ethics Approval: Not applicable.

Conflicts of Interest: The authors declare no conflicts of interest.

References

1. Rogers JA, Someya T, Huang Y. Materials and mechanics for stretchable electronics. Science. 2010;327(5973):1603–7. doi:10.1126/science.1182383.
2. Li B, Cao YP, Feng XQ, Gao H. Mechanics of morphological instabilities and surface wrinkling in soft materials: a review. Soft Matter. 2012;8(21):5728–45. doi:10.1039/c2sm00011c.
3. Basu SK, Bergstreser AM, Francis LF, Scriven LE, McCormick AV. Wrinkling of a two-layer polymeric coating. J Appl Phys. 2005;98(6):063507. doi:10.1063/1.2043255.
4. Hong W, Zhao X, Zhou J, Suo Z. A theory of coupled diffusion and large deformation in polymeric gels. J Mech Phys Solids. 2008;56(5):1779–93. doi:10.1016/j.jmps.2007.11.010.
5. Zhang XX, Guo TF, Zhang YW. Instability analysis of a programmed hydrogel plate under swelling. J Appl Phys. 2011;109(6):063527. doi:10.1063/1.3565060.
6. Ding W, Yang Y, Zhao Y, Jiang S, Cao Y, Lu C. Well-defined orthogonal surface wrinkles directed by the wrinkled boundary. Soft Matter. 2013;9(14):3720–6. doi:10.1039/c2sm27359d.
7. Yin J, Cao Z, Li C, Sheinman I, Chen X. Stress-driven buckling patterns in spheroidal core/shell structures. Proc Natl Acad Sci USA. 2008;105(49):19132–5. doi:10.1073/pnas.0810443105.
8. Yin J, Chen X, Sheinman I. Anisotropic buckling patterns in spheroidal film/substrate systems and their implications in some natural and biological systems. J Mech Phys Solids. 2009;57(9):1470–84. doi:10.1016/j.jmps.2009.06.002.
9. Li B, Cao YP, Feng XQ, Gao H. Surface wrinkling of mucosa induced by volumetric growth: theory, simulation and experiment. J Mech Phys Solids. 2011;59(4):758–74. doi:10.1016/j.jmps.2011.01.010.
10. Ciarletta P, Ben Amar M. Pattern formation in fiber-reinforced tubular tissues: folding and segmentation during epithelial growth. J Mech Phys Solids. 2012;60(3):525–37. doi:10.1016/j.jmps.2011.11.004.
11. Wu B, Kong L, Chen W, Riccobelli D, Destrade M. Electro-mechanical wrinkling of soft dielectric films bonded to hyperelastic substrates. J Mech Phys Solids. 2026;209:106490. doi:10.1016/j.jmps.2025.106490.
12. Oguntade E, Wigham C, Owuor L, Aryal U, O'Grady K, Acierto A, et al. Dry and wet wrinkling of a silk fibroin biopolymer by a shape-memory material with insight into mechanical effects on secondary structures in the silk network. J Mater Chem B. 2024;12(26):6351–70. doi:10.1039/d4tb00112e.
13. Webber JJ, Worster MG. Wrinkling instabilities of swelling hydrogels. Phys Rev E. 2024;109(4):044602. doi:10.1103/physreve.109.044602.
14. Veldin T, Trojer J, Brank B, Brojan M. Wrinkling of thin plates and shells on shrinking substrates. Thin Walled Struct. 2025;215:113504. doi:10.1016/j.tws.2025.113504.
15. Shen J, Fu Y, Pirrera A, Groh RMJ. Wrinkling of differentially growing bilayers with similar film and substrate moduli. J Mech Phys Solids. 2024;193:105900. doi:10.1016/j.jmps.2024.105900.
16. Huang R. Kinetic wrinkling of an elastic film on a viscoelastic substrate. J Mech Phys Solids. 2005;53(1):63–89. doi:10.1016/j.jmps.2004.06.007.
17. Montanari M, Hamaied R, Gao C, Bertolin C, Spagnoli A. An exploration into surface wrinkling in 3D printing inspired orthotropic bilayer systems. Int J Solids Struct. 2024;298:112862. doi:10.1016/j.ijsolstr.2024.112862.
18. Guan X, Nguyen N, Pocivavsek L, Cerda E, Velankar SS. Flat, wrinkled, or ridged: relaxation of an elastic film on a viscous substrate undergoing continuous compression. Int J Solids Struct. 2023;275:112242. doi:10.1016/j.ijsolstr.2023.112242.

19. Yuan X, Zhao P, Fan Q, Wang Y, Li X. Theoretical and numerical analysis on buckling instability in a thin film sandwiched between two finite-thickness substrates under in-plane compression. Int J Solids Struct. 2024;304:113037. doi:10.1016/j.ijsolstr.2024.113037.
20. Nagashima S, Okamoto R, Matsubara S, Okumura D. Soft wetting of film-substrate bilayers: wrinkle flattening near the three-phase contact line. Int J Multiph Flow. 2025;191(1):105324. doi:10.1016/j.ijmultiphaseflow.2025.105324.
21. Huang ZY, Hong W, Suo Z. Nonlinear analyses of wrinkles in a film bonded to a compliant substrate. J Mech Phys Solids. 2005;53(9):2101–18. doi:10.1016/j.jmps.2005.03.007.
22. Audoly B, Boudaoud A. Buckling of a stiff film bound to a compliant substrate-Part I:: formulation, linear stability of cylindrical patterns, secondary bifurcations. J Mech Phys Solids. 2008;56(7):2401–21. doi:10.1016/j.jmps.2008.03.003.
23. Cai S, Breid D, Crosby AJ, Suo Z, Hutchinson JW. Periodic patterns and energy states of buckled films on compliant substrates. J Mech Phys Solids. 2011;59(5):1094–114. doi:10.1016/j.jmps.2011.02.001.
24. Kordolemis A, Giannakopoulos AE. Wrinkling analysis of a stiff shallow film mounted on a cylindrically curved compliant substrate, Part II: checkerboard and hexagonal modes. Int J Solids Struct. 2025;317:113383. doi:10.1016/j.ijsolstr.2025.113383.
25. Jia F, Ben Amar M. Theoretical analysis of growth or swelling wrinkles on constrained soft slabs. Soft Matter. 2013;9(34):8216–26. doi:10.1039/c3sm50640a.
26. Breid D, Crosby AJ. Effect of stress state on wrinkle morphology. Soft Matter. 2011;7(9):4490–6. doi:10.1039/c1sm05152k.
27. Pandurangi SS, Akerson A, Elliott RS, Healey TJ, Triantafyllidis N. Nucleation of creases and folds in hyperelastic solids is not a local bifurcation. J Mech Phys Solids. 2022;160(1):104749. doi:10.1016/j.jmps.2021.104749.
28. Li M, Sun B. Post-buckling behaviors of thin-film soft-substrate bilayers with finite-thickness substrate. Sci Rep. 2022;12(1):4074. doi:10.1038/s41598-022-08136-w.
29. Brau F, Damman P, Diamant H, Witten TA. Wrinkle to fold transition: influence of the substrate response. Soft Matter. 2013;9(34):8177–86.
30. Xie WH, Huang X, Cao YP, Li B, Feng XQ. Buckling and postbuckling of stiff lamellae in a compliant matrix. Compos Sci Technol. 2014;99(6):89–95. doi:10.1016/j.compscitech.2014.05.015.
31. Wang JW, Li B, Cao YP, Feng XQ. Surface wrinkling patterns of film–substrate systems with a structured interface. J Appl Mech. 2015;82(5):051009. doi:10.1115/1.4030010.
32. Cerda E, Mahadevan L. Geometry and physics of wrinkling. Phys Rev Lett. 2003;90(7):074302. doi:10.1103/physrevlett.90.074302.
33. Ben Amar M, Goriely A. Growth and instability in elastic tissues. J Mech Phys Solids. 2005;53(10):2284–319. doi:10.1016/j.jmps.2005.04.008.
34. Efimenko K, Rackaitis M, Manias E, Vaziri A, Mahadevan L, Genzer J. Nested self-similar wrinkling patterns in skins. Nat Mater. 2005;4(4):293–7. doi:10.1038/nmat1342.
35. Schweikart A, Fery A. Controlled wrinkling as a novel method for the fabrication of patterned surfaces. Microchim Acta. 2009;165(3):249–63. doi:10.1007/s00604-009-0153-3.
36. Kim P, Abkarian M, Stone HA. Hierarchical folding of elastic membranes under biaxial compressive stress. Nature Mater. 2011;10(12):952–7. doi:10.1038/nmat3144.
37. Nikravesh S, Ryu D, Shen YL. Direct numerical simulation of buckling instability of thin films on a compliant substrate. Adv Mech Eng. 2019;11(4):1687814019840470. doi:10.1177/1687814019840470.
38. Ryu D, Mongare A. Corrugated photoactive thin films for flexible strain sensor. Materials. 2018;11(10):1970. doi:10.3390/ma11101970.
39. Lipomi DJ, Tee BC, Vosgueritchian M, Bao Z. Stretchable organic solar cells. Adv Mater. 2011;23(15):1771–5. doi:10.1002/adma.201004426.
40. Cao YP, Zheng XP, Li B, Feng XQ. Determination of the elastic modulus of micro- and nanowires/tubes using a buckling-based metrology. Scr Mater. 2009;61(11):1044–7. doi:10.1016/j.scriptamat.2009.08.023.
41. Kim DH, Viventi J, Amsden JJ, Xiao J, Vigeland L, Kim YS, et al. Dissolvable films of silk fibroin for ultrathin conformal bio-integrated electronics. Nat Mater. 2010;9(6):511–7. doi:10.1038/nmat2745.

42. Zhao L, Xu M, Hong X, Chen J, Mei C, Li X, et al. Sandpaper-induced wrinkled PDMS/nanosilica membrane for assembling AgNWs and PEDOT: PSS stretchable transparent electrodes. Langmuir. 2025;41(45):30370–81. doi:10.1021/acs.langmuir.5c04016.
43. Lee G, Zarei M, Wei Q, Zhu Y, Lee SG. Surface wrinkling for flexible and stretchable sensors. Small. 2022;18(42):2203491. doi:10.1002/smll.202203491.
44. Li L, Zheng Y, Liu E, Zhao X, Yu S, Wang J, et al. Stretchable and ultrasensitive strain sensor based on a bilayer wrinkle-microcracking mechanism. Chem Eng J. 2022;437:135399. doi:10.1016/j.cej.2022.135399.
45. Dimmock RL, Wang X, Fu Y, El Haj AJ, Yang Y. Biomedical applications of wrinkling polymers. Recent Prog Mater. 2020;2(1):1–31. doi:10.21926/rpm.2001005.
46. Watanabe M, Tazawa H, Suganuma K. Preparation of drug microparticles with a narrow size distribution using regular dimples induced by buckling instability. Appl Surf Sci. 2021;563(6):150251. doi:10.1016/j.apsusc.2021.150251.
47. Chan EP, Crosby AJ. Fabricating microlens arrays by surface wrinkling. Adv Mater. 2006;18(24):3238–42. doi:10.1002/adma.200601595.
48. Gabardo CM, Yang J, Smith NJ, Adams-McGavin RC, Soleymani L. Programmable wrinkling of self-assembled nanoparticle films on shape memory polymers. ACS Nano. 2016;10(9):8829–36. doi:10.1021/acsnano.6b04584.
49. Stafford CM, Harrison C, Beers KL, Karim A, Amis EJ, VanLandingham MR, et al. A buckling-based metrology for measuring the elastic moduli of polymeric thin films. Nat Mater. 2004;3(8):545–50. doi:10.1038/nmat1175.
50. Kim DH, Rogers JA. Stretchable electronics: materials strategies and devices. Adv Mater. 2008;20(24):4887–92. doi:10.1002/adma.200801788.
51. Guvendiren M, Yang S, Burdick JA. Swelling-induced surface patterns in hydrogels with gradient crosslinking density. Adv Funct Mater. 2009;19(19):3038–45. doi:10.1002/adfm.200900622.
52. Feng D, Su X, Chen R, Chen H, Yang Y, Lu S, et al. Innovative wrinkle fabrication on polymer surfaces: applications in optics and anti-counterfeiting. Nano Today. 2025;65:102843. doi:10.1016/j.nantod.2025.102843.
53. Rahmawan Y, Chen CM, Yang S. Recent advances in wrinkle-based dry adhesion. Soft Matter. 2014;10(28):5028–39. doi:10.1039/c4sm00027g.
54. Genzer J, Groenewold J. Soft matter with hard skin: from skin wrinkles to templating and material characterization. Soft Matter. 2006;2(4):310–23.
55. Song J, Jiang H, Choi WM, Khang DY, Huang Y, Rogers JA. An analytical study of two-dimensional buckling of thin films on compliant substrates. J Appl Phys. 2008;103(1):014303. doi:10.1063/1.2828050.
56. Bowden N, Brittain S, Evans AG, Hutchinson JW, Whitesides GM. Spontaneous formation of ordered structures in thin films of metals supported on an elastomeric polymer. Nature. 1998;393(6681):146–9. doi:10.1038/30193.
57. Huck WTS, Bowden N, Onck P, Pardoen T, Hutchinson JW, Whitesides GM. Ordering of spontaneously formed buckles on planar surfaces. Langmuir. 2000;16(7):3497–501. doi:10.1021/la991302l.
58. Allen HG. Analysis and design of structural sandwich panels. Oxford, UK: Pergamon Press Ltd.; 1969.
59. Volynskii AL, Bazhenov S, Lebedeva OV, Bakeev NF. Mechanical buckling instability of thin coatings deposited on soft polymer substrates. J Mater Sci. 2000;35(3):547–54. doi:10.1023/A:1004707906821.
60. Zhang S, Sun D, Fu Y, Du H. Toughness measurement of thin films: a critical review. Surf Coat Technol. 2005;198(1–3):74–84. doi:10.1016/j.surfcoat.2004.10.021.
61. Brau F, Vandeparre H, Sabbah A, Poulard C, Boudaoud A, Damman P. Multiple-length-scale elastic instability mimics parametric resonance of nonlinear oscillators. Nat Phys. 2011;7(1):56–60. doi:10.1038/nphys1806.
62. Hure J, Roman B, Bico J. Stamping and wrinkling of elastic plates. Phys Rev Lett. 2012;109(5):054302. doi:10.1103/physrevlett.109.054302.
63. Wang Q, Zhao X. A three-dimensional phase diagram of growth-induced surface instabilities. Sci Rep. 2015;5(1):8887. doi:10.1038/srep08887.
64. Jiang H, Khang DY, Song J, Sun Y, Huang Y, Rogers JA. Finite deformation mechanics in buckled thin films on compliant supports. Proc Natl Acad Sci U S A. 2007;104(40):15607–12. doi:10.1073/pnas.0702927104.
65. Arafat Y, Dutta I, Panat R. Super-stretchable metallic interconnects on polymer with a linear strain of up to 100%. Appl Phys Lett. 2015;107(8):081906. doi:10.1063/1.4929605.

66. Lipomi DJ, Vosgueritchian M, Tee BC, Hellstrom SL, Lee JA, Fox CH, et al. Skin-like pressure and strain sensors based on transparent elastic films of carbon nanotubes. Nat Nanotech. 2011;6(12):788–92. doi:10.1038/nnano.2011.184.
67. Sekitani T, Nakajima H, Maeda H, Fukushima T, Aida T, Hata K, et al. Stretchable active-matrix organic light-emitting diode display using printable elastic conductors. Nat Mater. 2009;8(6):494–9. doi:10.1038/nmat2459.
68. Kayser LV, Lipomi DJ. Stretchable conductive polymers and composites based on PEDOT and PEDOT: PSS. Adv Mater. 2019;31(10):1806133. doi:10.1002/adma.201806133.
69. Luo R, Li X, Li H, Du B, Zhou S. A stretchable and printable PEDOT: PSS/PDMS composite conductors and its application to wearable strain sensor. Prog Org Coat. 2022;162:106593. doi:10.1016/j.porgcoat.2021.106593.
70. Hutchinson JW. The role of nonlinear substrate elasticity in the wrinkling of thin films. Phil Trans R Soc A. 2013;371(1993):20120422. doi:10.1098/rsta.2012.0422.
71. Vella D, Bico J, Boudaoud A, Roman B, Reis PM. The macroscopic delamination of thin films from elastic substrates. Proc Natl Acad Sci USA. 2009;106(27):10901–6. doi:10.1073/pnas.0902160106.
72. Bi H, Li W, Wang L, Wang B. Numerical investigation of dynamic wrinkling behaviors in stiff-film/PDMS-substrate structure. Polymers. 2026;18(2):292. doi:10.3390/polym18020292.
73. Graz IM, Cotton DPJ, Lacour SP. Extended cyclic uniaxial loading of stretchable gold thin-films on elastomeric substrates. Appl Phys Lett. 2009;94(7):071902. doi:10.1063/1.3076103.
74. Sekitani T, Noguchi Y, Hata K, Fukushima T, Aida T, Someya T. A rubberlike stretchable active matrix using elastic conductors. Science. 2008;321(5895):1468–72. doi:10.1126/science.1160309.
75. Groenewold J. Wrinkling of plates coupled with soft elastic media. Phys A Stat Mech Appl. 2001;298(1–2):32–45. doi:10.1016/s0378-4371(01)00209-6.
76. Erfanian Nazif Toosi M, Alinia Y. Wrinkling instability of a thin film deposited on a graded interlayer/substrate system. Acta Mech. 2025;236(9):4921–37. doi:10.1007/s00707-025-04389-4.
77. Chung JY, Nolte AJ, Stafford CM. Surface wrinkling: a versatile platform for measuring thin-film properties. Adv Mater. 2011;23(3):349–68. doi:10.1002/adma.201001759.
78. Shan Y, Wang L, Wu W. Post-buckling analysis of square film under in-plane torsion: experiment and simulation comparisons. Acta Mech Sin. 2025;42(1):424609. doi:10.1007/s10409-024-24609-x.
79. Yang J, Damle S, Maiti S, Velankar SS. Stretching-induced wrinkling in plastic-rubber composites. Soft Matter. 2017;13(4):776–87. doi:10.1039/c6sm01823h.
80. Nikravesh S, Ryu D, Shen YL. Surface instability of composite thin films on compliant substrates: direct simulation approach. Front Mater. 2019;6:214. doi:10.3389/fmats.2019.00214.
81. Nikravesh S, Ryu D, Shen YL. Instabilities of thin films on a compliant substrate: direct numerical simulations from surface wrinkling to global buckling. Sci Rep. 2020;10(1):5728. doi:10.1038/s41598-020-62600-z.
82. Shen YL, Nikravesh S, Anan AR, Ryu D. Predicting wrinkle formation in flexible thin-film structures. In: Proceedings of the 2024 19th International Microsystems, Packaging, Assembly and Circuits Technology Conference (IMPACT); 2024 Oct 22–25; Taipei, China. p. 69–72. doi:10.1109/impact63555.2024.10818912.
83. Al Rifat Anan M, Ryu D, Shen YL. Wrinkle formation in cylindrical thin film-compliant core structures: numerical simulations and effects of inelastic deformation. Adv Mech Eng. 2025;17(5):16878132251342041. doi:10.1177/16878132251342041.
84. Nikravesh S, Ryu D, Shen YL. Direct numerical simulations of three-dimensional surface instability patterns in thin film-compliant substrate structures. Sci Rep. 2021;11(1):16449. doi:10.1038/s41598-021-95414-8.
85. Nikravesh S, Ryu D, Shen YL. Surface wrinkling versus global buckling instabilities in thin film-substrate systems under biaxial loading: direct 3D numerical simulations. Adv Theory Simul. 2022;5(9):2200183. doi:10.1002/adts.202200183.
86. Luo XM, Zhang GP. Deformation-mechanism dependent stretchability of nanocrystalline gold films on flexible substrates. J Mater Res. 2017;32(18):3516–23. doi:10.1557/jmr.2017.349.
87. Pamulaparthi Venkata S, Fu Y, Fu Y, Danesh H, Destrade M, Balbi V. Wrinkling instability of 3D auxetic bilayers in tension. J Mech Phys Solids. 2025;204:106301. doi:10.1016/j.jmps.2025.106301.

88. Gao F, Yao Y, Liu T. Tension-induced localized wrinkling in a patched thin film supported by an elastomer. Langmuir. 2024;40(1):133–40. doi:10.1021/acs.langmuir.3c02282.
89. Qiu X, Guo J, Wang C, Tan H. Stretch-induced wrinkling and post-buckling bifurcation in rectangular films: insights into energy barrier mechanisms. Int J Mech Sci. 2025;299:110398. doi:10.1016/j.ijmecsci.2025.110398.
90. Shen YL. Constrained deformation of materials: devices, heterogeneous structures and thermo-mechanical modeling. Boston, MA, USA: Springer; 2010. doi:10.1007/978-1-4419-6312-3.
91. Tahk D, Lee HH, Khang DY. Elastic moduli of organic electronic materials by the buckling method. Macromolecules. 2009;42(18):7079–83. doi:10.1021/ma900137k.
92. Chen X, Hutchinson JW. A family of herringbone patterns in thin films. Scr Mater. 2004;50(6):797–801. doi:10.1016/j.scriptamat.2003.11.035.